Finite Element Modeling of Hard Roller Burnishing: An Analysis on the Effects of Process Parameters Upon Surface Finish and Residual Stresses

Article *in* Journal of Manufacturing Science and Engineering · August 2007

DOI: 10.1115/1.2738121

CITATIONS
43

READS
757

4 authors, including:

Partchapol Sartkulvanich
The Ohio State University
13 PUBLICATIONS **327** CITATIONS

SEE PROFILE

Ciro A Rodriguez
Tecnológico de Monterrey
87 PUBLICATIONS **1,009** CITATIONS

SEE PROFILE

Finite Element Modeling of Hard Roller Burnishing: An Analysis on the Effects of Process Parameters Upon Surface Finish and Residual Stresses

Partchapol Sartkulvanich

Taylan Altan
e-mail: Altan.1@osu.edu

Engineering Research Center for Net Shape Manufacturing,
The Ohio State University,
Columbus, OH 43210

Francisco Jasso

Ciro Rodriguez

Center for Innovation in Design and Technology,
Instituto Tecnológico y de Estudios Superiores de Monterrey,
Monterrey, N.L., Mexico

Hard roller burnishing is a cost-effective finishing and surface enhancement process where a ceramic ball rolls on the machined surface to flatten the roughness peaks. The ball is supported and lubricated by hydrostatic fluid in a special tool holder. The process not only improves surface finish but also imposes favorable compressive residual stresses in functional surfaces, which can lead to long fatigue life. Most research in the past focused on experimental studies. There is still a special need for a reliable finite element method (FEM) model that provides a fundamental understanding of the process mechanics. In this study, two-dimensional (2D) and three-dimensional FEM models for hard roller burnishing were established. The developed 2D FEM model was used to study the effects of process parameters (i.e., burnishing pressure, feed rate) on surface finish and residual stresses. The simulation results were evaluated and compared to the experimental data. Results show that the established FEM model could predict the residual stresses and provided useful information for the effect of process parameters. Both FEM and experiments show that burnishing pressure is the most influence, where high burnishing pressure produces less roughness and more compressive residual stress at the surface.
[DOI: 10.1115/1.2738121]

Keywords: finite element, roller burnishing, surface finish, residual stress

1 Introduction

The surface integrity of an engineered surface is generally characterized in terms of surface finish, state of residual stress, microstructure, and microhardness. Generally, good surface finish, high compressive residual stress, and high hardness of the surface layer prolong the fatigue life of the components. The development of hard turning technology makes it possible to replace at least some rough grinding with single-point cutting processes. However, the application of hard turning as a finishing process is still limited by tool wear. To broaden the capability of hard turning as a finishing process, roller burnishing could be used since a burnishing tool can be installed on the same machine setting and the process can improve surface quality (i.e., by providing good surface finish and converting tensile residual stresses to compressive).

Figure 1 illustrates a typical roller burnishing operation. The process is characterized by a single pass of a smooth free-rolling spherical ball (3–12 mm dia) under a normal force that is sufficient to deform the roughness peaks of the surface profile. The ball is in contact only with the surface to be burnished and free to roll with very low friction. As in the cutting action, small plastic deformation is produced over the entire surface as the tool continuously feeds along the workpiece axis.

To implement a successful hard roller burnishing process, the effects of burnishing parameters on the surface finish and surface integrity need to be evaluated. Most of research in the past focused on experimental studies. However, there is still a special need for reliable finite element method (FEM) simulation models that provide a fundamental understanding of the process and help in optimizing burnishing conditions.

The objectives of this study are to (i) establish an FEM model for roller burnishing to study the effects of roller burnishing parameters (i.e., burnishing pressure and feed rate) on surface roughness and residual stresses and (ii) validate the simulation results with results obtained from roller burnishing experiments. In this study, two-dimensional (2D) and three-dimensional (3D) FEM models of roller burnishing were further developed from previous work presented in [1]. Additional modifications include (i) determination of flow stress of the workpiece surface using instrumented ball indentation tests in conjunction with FEM inverse analysis, (ii) calibration of burnishing force by considering pressure loss during FEM simulations, (iii) consideration of initial surface roughness and residual stresses from hard turning experiments, and (iv) validation of FEM simulations with hard roller burnishing experiments.

2 Literature Review

In the past decades, research in roller burnishing was based on experimental studies. The research groups contributing to this field mainly include the WZL/RWTH, Aachen, Germany [2,3], Ecoroll, Germany [4], the University of Toledo [5] and Lambda Research [6]. Some experimental studies by other researchers have also been reported worldwide [7–10].

Experimental studies by Prevéy [11], Prevéy and Cammett [12], and Prevéy et al. [13–15] showed that parts finished by roller burnishing process had longer fatigue life compared to shot peened parts, for IN 718, Ti-6Al-4V, stainless steels, and Aluminum 7075-T6. Hassan and Al-Bsharat [16] and Hassan and Maqableh [17] had similar observations for nonferrous materials.

Contributed by the Manufacturing Science Division of ASME for publication in the JOURNAL OF MANUFACTURING SCIENCE AND ENGINEERING. Manuscript received July 19, 2006; final manuscript received February 16, 2007. Review conducted by Albert J. Shih.

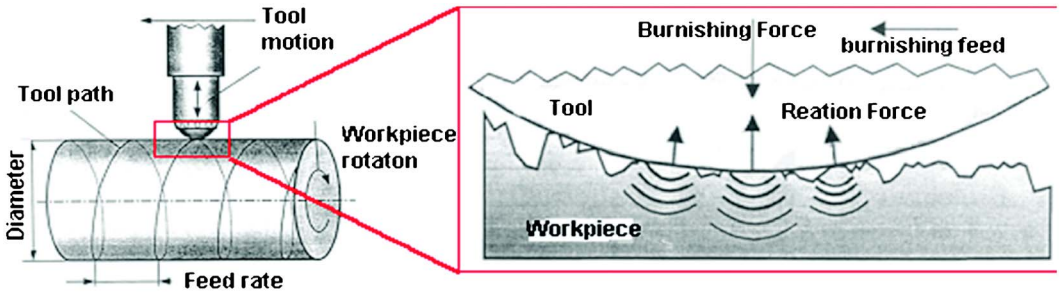

Fig. 1 Roller burnishing process [2]

Experiments on 100Cr6 (or AISI 52100) bearing steel, conducted by Röttger [2] and Klocke and Liermann [3], showed that roller burnishing not only improved the surface roughness but also converted tensile residual stress previously produced by hard turning with worn inserts into compressive residual stress on the surface.

The process parameters in roller burnishing generally include burnishing speed v_b, burnishing feed rate f_b, applied fluid pressure P_b or normal force F_b, and ball diameter d_b. For hard roller burnishing (hard turning plus roller burnishing), experiments indicate that nearly constant surface roughness can be achieved over a wide range of process conditions [3]. In a recent study conducted by Röttger [2], 100Cr6V samples (equivalent to AISI 52100) were first hardened, hard turned using tools with different amount of flank wear, and then burnished using different burnishing conditions.

The following conclusions were drawn from Röttger's study [2]:

- Surface finish could be improved up to 70% by means of increasing burnishing pressure and decreasing workpiece hardness
- The improvement of surface finish was not sensitive to (*a*) burnishing speed and (*b*) feed rate in the low range
- High burnishing pressure and large ball diameter caused the surface residual stress to be more compressive with an increased penetration depth
- Different initial residual stress distributions generated by hard turning did not significantly influence the residual stress behavior after roller burnishing
- Burnishing pressures higher than 20 MPa result in an increase of surface hardness

A number of predictive models have been developed in order to estimate surface properties for a given set of roller burnishing conditions. The modeling of roller burnishing was classified in three different categories, i.e., analytical, statistical, and FEM models. Hassan et al. [18] developed a statistical model by using response surface model to fit experimental roller burnishing force and number of tool passes with the mean roughness. El-Axir and El-Khabeery [8] developed statistical models to predict the surface roughness and microhardness using design of experiments (DOE) technique and a set of experimental data obtained from roller burnishing tests on St-37 steel samples.

Bouzid et al. [19] developed an equation to determine the roughness depth after burnishing, based on geometries of the tool and surface roughness of the workpiece. A very small burnishing force (150 N) was used. Bouzid used Hertz theory for contact of two elastic objects (sphere-to-cylinder contact) to calculate the penetration depth, which was later used to subtract initial roughness depth to estimate the burnished roughness. However, Bouzid studied only the case for which the penetration depth is smaller than the initial surface roughness, while the machined surface was assumed to be flat (no initial roughness) when calculating the penetration depth. Black et al. [20] developed equations using the slip-line theory to determine factors such as the energy required for burnishing process, the depth of the deformed surface layer and the states of stress and strain induced in this layer as functions of the burnishing tool geometry, the applied force, the workpiece material properties, and the friction conditions at the tool/workpiece interface. Black's simplified 2D plane strain model was established such that a wedge-shaped tool was sliding over the workpiece surface [20]. A rigid-perfectly plastic material was assumed.

Skalski et al. [21] developed a 2D quasi-static burnishing model to numerically analyze the relations between the tool force, penetration depth, radius of the contact area, and depth of plastic deformation under different tool radii and workpiece yield strengths. The model used axisymmetric formulation and assumed that the tool was rigid and the workpiece was elastic-plastic with strain hardening. The results from Skalski's study [21] showed that the force acting on the tool was mainly influenced by the tool radius rather than the yield strength of the material. Bouzid and Saï [22] developed a 3D FEM model, while considering the elastic-plastic properties of the workpiece, to calculate the ball penetration depth. However, the geometry-based equation to determine the roughness depth by Bouzid et al. [19] was still used and the model did not consider initial surface roughness and the effect of burnishing feed.

Röttger [2] developed a 2D FEM model for roller burnishing using a commercial FEM software DEFORM™-2D. In this model (Fig. 2), a rigid ball was at intermediate position at the start and then pressed down on the rough workpiece surface until the reaction force reached a predefined value that is equal to the applied burnishing force. Consequently, the ball was lifted up from the surface and moved horizontally by the distance of the burnishing feed. This process was then repeated for four cycles. However, this force-control model underestimated the ball penetration depth

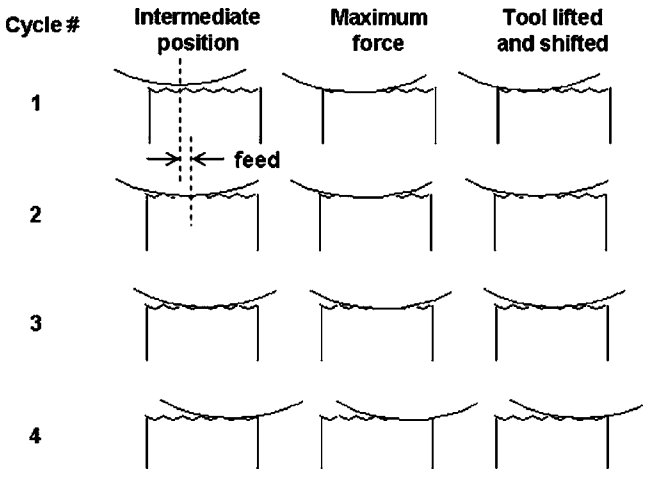

Fig. 2 Simulation sequence for 2-D FEM modeling of roller burnishing [2]

Table 1 Machine, tools, and process conditions used in hard turning and roller burnishing experiments

Hard Turning Experiments		
Machine tool	CNC Hardinge Lathe, "Quest" Model (with hydrostatic linear guideway and maximum spindle speed of 15,000 rpm)	
Cutting tool	Tool Holder	Kennametal (AISI MDJNL 124B) Side rake angle=−5 deg Back rake angles=−5 deg Lead angle=−32 deg Included angle=55 deg
	Cutting insert	Kennametal (DNGA432T0820, Grade: K090) A composite (Black) ceramic, composed of Alumina and 30% TiC Included angle=55 deg
Cutting condition	Cutting speed=122 m/min Cutting feed rate=0.1 mm/rev Depth of cut=0.127 mm	
Hard Roller Burnishing Experiments		
Hydraulic pump	Ecoroll HGP 4.3 Maximum pressure of 400 bar (or 40 MPa) Electricity requirement of 400 V, 50 Hz	
Hard roller burnishing tools	Ecoroll HG 6 Ceramic ball tool, 6 mm diam Tool holder with 15 deg contact angle	
Burnishing condition	Burnishing pressure (P_b)=32, 36, 40 MPa Burnishing feed rate (f_b)=0.02, 0.05, 0.08 mm/rev Burnishing speed (v_b)=150 m/min	

because of line contact (due to the plane strain condition) and unrealistic workpiece width (as well as the width of a contact area) that was fixed to be 1 mm.

3 Hard Turning and Hard Roller Burnishing Experiments

Hard turning and hard roller burnishing experiments were conducted at Hardinge Inc. Measurements of surface roughness and hardness were performed at the ERC/NSM, whereas the measurements of residual stresses on machined/ burnished surfaces were conducted by the Timken Company.

Workpiece samples used for hard turning and burnishing experiments were cylindrical bars (50 mm dia × 150 mm length), made of AISI 52100 bearing steel. Samples were through-hardened to obtain a surface hardness of 58-60 HRC prior to hard turning.

A Hardinge CNC lathe "Quest Model" was used for both hard turning and hard roller burnishing experiments. Technical information of CNC machine and tools used in hard turning and burnishing experiments are shown in Table 1. Ecoroll burnishing equipment, consisting of hydraulic pump and ceramic ball tool, were used in hard roller burnishing experiments. Hard turning tests were conducted using only one cutting condition for which an equivalent machined surface roughness could be generated. For hard roller burnishing tests, process parameters used are shown in Table 1 (burnishing pressures, feeds, and speeds). The ranges of burnishing process parameters were suggested by the burnishing tool supplier, Ecoroll Company.

Roughness parameters, namely, roughness depth R_z and mean roughness R_a, were measured with a "Stylus" mechanical surface analyzer manufactured by Federal Company. A stylus is a conical diamond; with 10 μm tip radius. Vertical resolution of the surface analyzer ranges from 0.002 μm to 0.010 μm (based on assigned length of measurement). Several measuring lengths (1–3 mm) have been tried out in order to obtain consistent surface roughness data. The measured roughness parameters were also compared to other experimental data by Röttger [2] and Luca [5]. Comparison shows that these roughness data are in the same range. Surface roughness measurements were preformed on all hard turned and burnished surfaces of the samples.

Residual stresses were measured in axial ($\sigma_{r,a}$) and tangential ($\sigma_{r,t}$) directions of the cylindrical workpiece, using the x-ray-diffraction technique, at the Timken Company. The conditions used for x-ray-diffraction measurements are listed in Table 2. Briefly, an x-ray tube generator operated at 52.5 kW to produce Cr $K\alpha$ radiation. The {2 1 1} reflection from the ferritic peak was used to measure elastic strains. Triaxial stress analysis was conducted for the selected surfaces using specimen tilt angles of 0 deg, 18.4 deg, 26.6 deg, 33.2 deg, 39.2 deg, and 45 deg. Residual stress measurements were conducted for the depths of 0 mm, 0.05 mm, 0.1 mm, 0.2 mm, 0.3 mm, and 0.4 mm from the workpiece surface. Only four surfaces were selected for measurements, including (i) hard turned surface, (ii) burnished surface with P_b=40 MPa, f_b=0.05 mm/rev, (iii) burnished surface with P_b=32 MPa, f_b=0.05 mm/rev, and (iv) burnished surface with P_b=40 MPa, f_b=0.02 mm/rev. Maximum residual stress resolu-

Table 2 Conditions used in the x-ray measurement of residual stresses

	X-ray diffraction conditions
Characteristic x-ray	Cr $K\alpha$
Power	52.5 W, 35 kV, 1.5 mA
Diffraction plane	{2 1 1}
Collimator diameter	3 mm
Specimen tilt angles (deg)	0, 18.4, 26.6, 33.2, 39.2, and 45
Stress constant	Carbon steel stress
X-ray line width (FWHM) (deg)	3.98–5.35
Resolution (MPa)	±9.4–±84.9

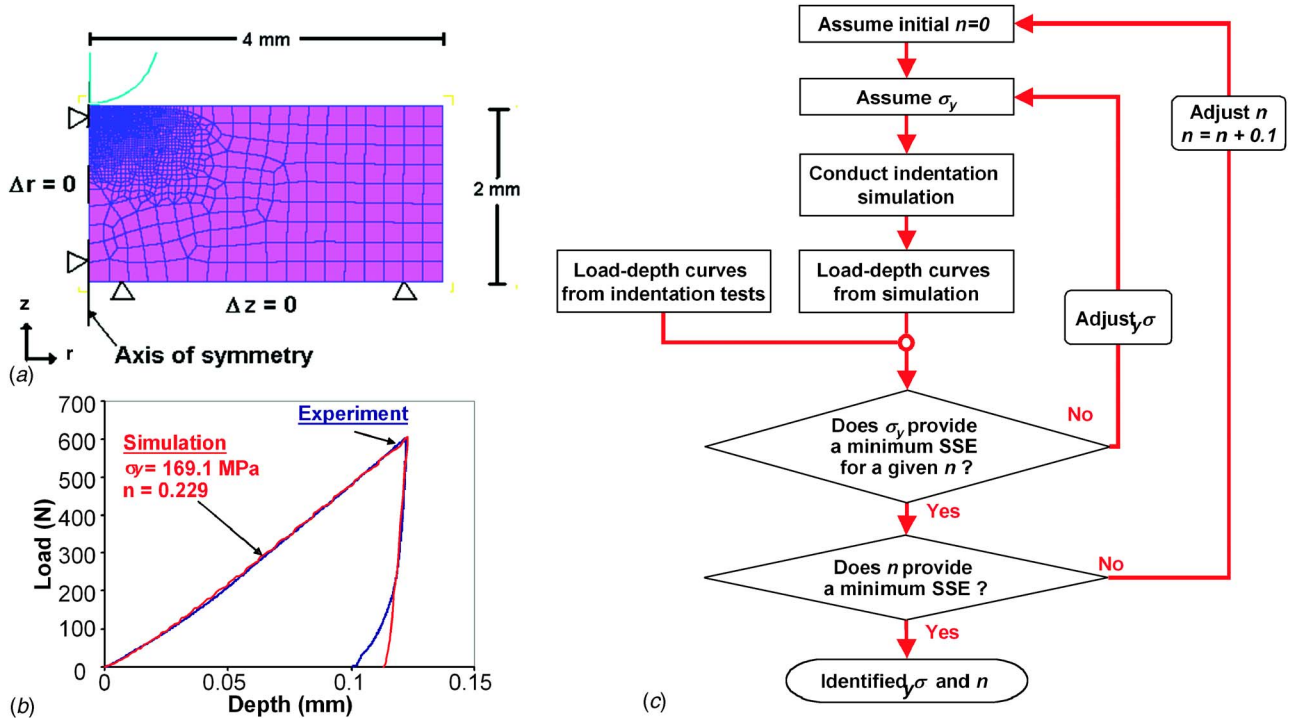

Fig. 3 (*a*) **Comparison of the load-depth curve between FEM simulation and indentation tests of the hard-turned AISI 52100 (60 HRC) and** (*b*) **comparison of the flow stress obtained from inverse analysis and compression tests [2,24]**

tion is within ±84.9 MPa. Experimental surface roughness and residual stress data were used for comparisons to the results obtained from FEM simulations.

4 Finite Element Modeling of Roller Burnishing Process

4.1 Flow Stress Determination for Hard Turned Surface. The flow stress at the machined surface of the workpiece (before roller burnishing) may differ from the bulk properties of the workpiece material due to large plastic deformations and possible phase transformations generated during machining. Conventional testing methods, e.g., compression and tensile tests, can only determine the property for the bulk sample and not for the surface layer. In order to obtain the flow stress for roller burnishing simulations, instrumented indentation tests (IIT), and an FEM inverse analysis were used. Details of flow stress determination procedures are presented in details by Morris et al. [23] and briefly discussed here.

Indentation tests are conducted at Advanced Technology Corporation on the hard turned surface of the sample, using a 0.76 mm ball indenter to penetrate to the maximum depth of 0.07 mm. Load-depth curves were recorded, Fig. 3(*a*), during indentation. The procedure to determine the flow stress is a process of matching the predicted load-depth curve from FEM simulation of indentation to the experimental curve by systematically changing the values for yield stress σ_y and strain-hardening exponent n of the flow stress given in

$$\sigma = \sigma_y \left(1 + \frac{E}{\sigma_y}\epsilon_p\right)^n \tag{1}$$

where

σ=flow stress (MPa)
ε_p=plastic strain
σ_y=yield stress (MPa)
E=Young's modulus (MPa)
n=strain-hardening exponent

The inverse analysis procedure for determining the material parameters (σ_y, n) are given in Fig. 4(*c*). When the minimum error between experimental and calculated values is reached, the material parameters of the flow stress equation are identified. The proposed methodology has been applied to identify the flow stress parameters of the hard-turned surface, made of AISI 52100 bearing steel. The accuracy of inverse analysis was verified by (a) comparing load-depth curves predicted by FEM simulation and obtained from experiment and (b) comparing the flow stress data obtained from the developed inverse analysis to those determined with compression tests.

FEM simulation of spherical indentation test is shown in Fig. 4(*a*). Preliminary sensitivity analysis showed that the curvature of the load-depth curves is sensitive to strain hardening exponent while the maximum load is dependent on the yield stress of the flow stress equation. As seen in Fig. 4(*c*), first, an FEM simulation is run with a strain-hardening exponent of zero $(n=0)$ and an initial assumed value for yield stress. The simulated load-depth curve is compared to the experimental data at several different points using the sum-squared error (SSE). The SSE is minimized by changing the yield stress while keeping the strain-hardening exponent constant at zero. The procedure is repeated by using different constant strain-hardening exponents of 0.1, 0.2, 0.3, etc. The values of yield stress are again varied to obtain minimum SSE for the given strain-hardening exponent. The local minimum SSEs for different values of strain hardening exponents are plotted to find the best strain-hardening value that provide a global minimum SSE. At this global minimum error, the strain-hardening exponent and the yield stress can be considered as the flow stress parameters, representing the material property of the surface layer. The developed inverse analysis procedure was also tested on AA 6061-T6 flat sample. As shown in Fig. 4(*b*), the predicted load-curve matches well with the experimental curves.

This inverse analysis procedure was used to determine the flow

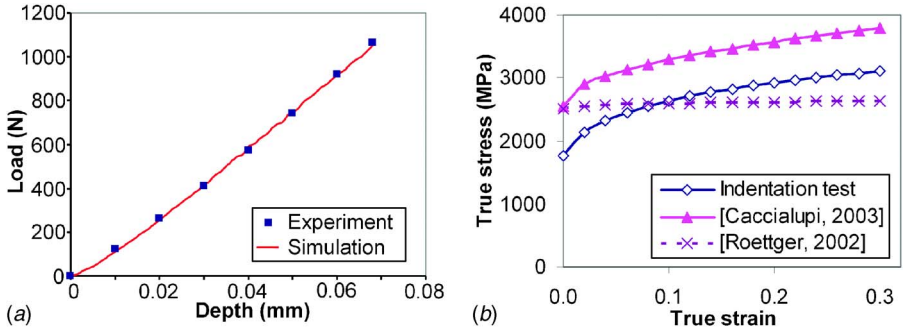

Fig. 4 (*a*) FEM simulation of indentation test, (*b*) comparison of load-depth curves between FEM simulation and experiment for indentation of AA 6061-T6, and (*c*) a flowchart of FEM inverse analysis to determine the flow stress of the surface material

stress of the hard-turned surface of AISI 52100 (60 HRC) sample. The predicted load-depth curve from FEM simulation matches the curve obtained from experiment (in Fig. 3(*a*)). The obtained flow stress equation has the yield stress (σ_y)=1765 MPa and the strain hardening exponent (n)=0.157, as shown in Eq. (2). Thus, for a hard turned AISI 52100 surface, (assuming that E=210 GPa for steel), the flow stress is given by Eq. (2). As shown in Fig. 3(*b*), the obtained flow stress data are comparable to those obtained from compression tests for the same sample material and initial hardness. The flow stress data obtained from inverse analysis have lower yield stress, but a strain hardening behavior similar to that of compression test data by Caccialupi [24]

$$\sigma = 1765(1 + 119\epsilon_p)^{0.157} \tag{2}$$

At room temperature, this flow stress equation is not strain-rate dependant. Therefore, the FEM model cannot consider the effects of burnishing speeds. However, according to many experimental studies, burnishing speed does not affect the process results [2,8].

4.2 FEM Modeling of Roller Burnishing. Although roller burnishing is a three-dimensional process, the use of 3D FEM model to analyze the effect of various process parameters on surface properties is limited, due to extremely large computational time required to run the simulation. Thus, the 2D FEM model is more practical and has yet the capability to study the effects of major burnishing parameters (i.e., burnishing pressure and burnishing feed) on surface finish and residual stresses.

In this study, FEM commercial software DEFORM™-2D is used. The procedure for modeling roller burnishing as a simplified 2D process is illustrated in Fig. 5 [1].

Figure 5(*a*) shows roller burnishing on a hard turned surface. Since the diameter of the workpiece sample is considerably larger than the diameter of the ball tool, the workpiece object is assumed to be flat. Plane (W) is assumed to pass through the center of the ball along one roughness ridge. Figure 5(*b*) shows the tool motion viewed on the section plane (W), which is assumed to pass through the ball's center aligned with one roughness ridge. Consider a material element located in front of the ball at the top of the roughness peak (A_0, subscript represents different times) in Fig. 5(*b*). As both the ball and workpiece rotate, this material element A_0 is rolled over by the ball and moves down vertically to the lowest position A_1 (A_0–A_1: loading). As the workpiece advances, this element then rises slightly due to elastic recovery of the surface and loses contact with the ball at the point A_2 (A_1–A_2: unloading). The vertical displacements of this element are projected onto a plane at the right window of Fig. 5(*b*). D represents the maximum penetration depth (or interface) of the ball between A_0 and A_1.

To simulate the deformation process for the material element moving from A_0 to A_2, the 3D rolling motion of the ball may be virtually transformed into a translational motion in Z direction in the proposed 2D model representing the projecting plane (small window in Fig. 5(*b*)). In this plane, the surface roughness profile generated by hard turning and the effect of burnishing feed rate can be implemented in the 2D FEM model. Steps of 2D simulation are described below and in Fig. 6.

Step 1. The ball moves down at a constant velocity to press on the workpiece.

Step 2. The ball stops at a certain maximum penetration depth (D).

Step 3. The ball unloads from the workpiece and return to its original position and shifts in the right direction about the distance of burnishing feed.

Step 4. The processes of loading/unloading/shift are repeated for 11 cycles.

Burnishing force (F_b) can be estimated analytically from the fluid pressure (P_b) that is applied to the ball tool and the ball diameter (d_b), and is given by

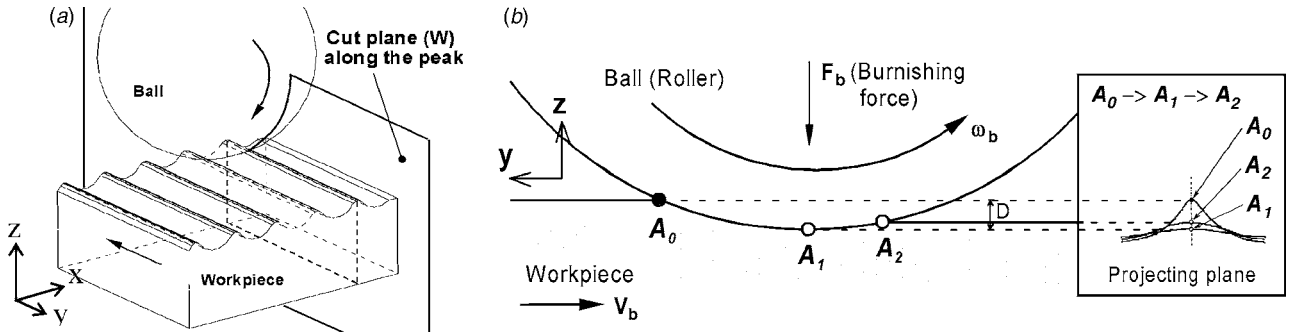

Fig. 5 (*a*) Roller burnishing process and (*b*) schematics of burnishing motion on the plane *W* [1]

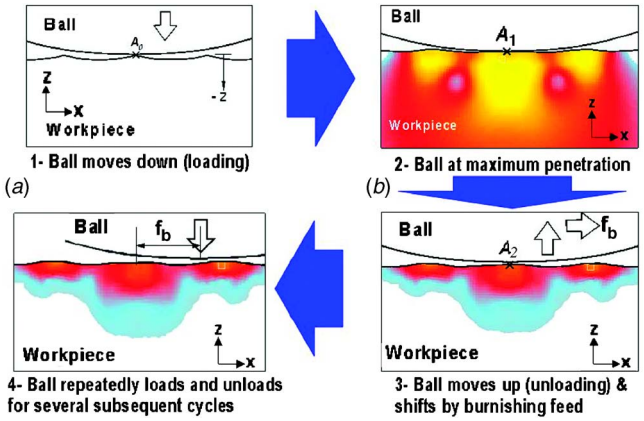

Fig. 6 Simulation sequence for 2D FEM modeling of roller burnishing

$$F_b = \frac{\pi}{4} d_b^2 P_b \tag{3}$$

For the same roller burnishing conditions and workpiece material, Röttger measured the burnishing forces by using a dynamometer on the tool holder fixture [2]. These experimental burnishing forces were compared to the theoretical forces calculated using Eq. (3). The comparison showed that the experimental forces are ~11% lower than the calculated forces. The differences are due to small fluid pressure loss along the circumferential gap between the ball and its socket. This percentage of force reduction due to pressure loss was taken into account in our 2D FEM model. As the experimental setup had a 15 deg contact angle (or the angle between the ball tool and the normal to workpiece surface), the burnishing force to be used in 2D roller burnishing simulations can be given by

$$F_b = 0.89 \frac{\pi}{4} d_b^2 P_b \cos(15 \text{ deg}) \tag{4}$$

In FEM model, the ball was considered as a rigid object and the workpiece was considered as an elastic-plastic object. Because pressurized fluid acts as coolant and lubricant in the process, isothermal condition and zero friction ($\mu=0$) were assumed. The displacement boundary constraints that were applied on the left, right and bottom boundaries of the workpiece are shown in Fig. 7.

The size of workpiece object in 2D FEM simulations was determined by conducting a sensitivity analysis for the effect of workpiece size on residual stresses and surface roughness. Preliminary 2D roller burnishing simulations were performed for only one indentation cycle (no feed effect) using different workpiece dimensions, i.e., 3×2 mm^2, 5×3.5 mm^2, 5×4.5 mm^2 and 7×6 mm^2. Analysis showed that the size of the workpiece strongly influenced the predicted results for both residual stress and surface roughness. However, the results did not change dramatically when the workpiece size was larger than 5×4.5 mm^2. Since the burnishing feed rate will need to be considered later in 2D roller burnishing simulations, the workpiece size was assumed to have larger dimensions, i.e., 7×6 mm^2.

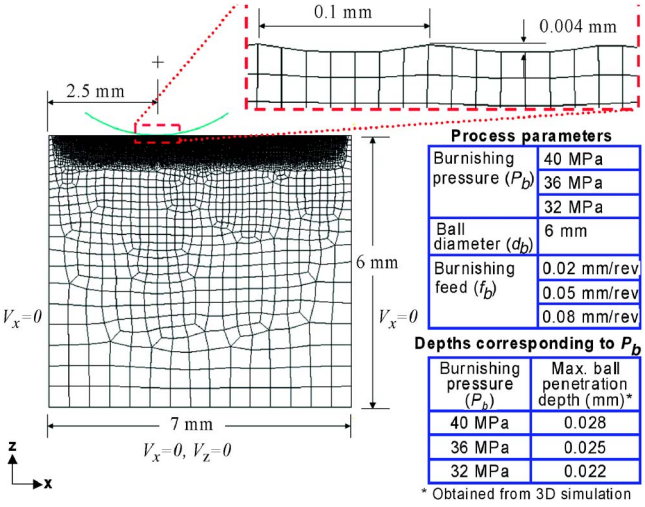

Fig. 7 Setups of the 2D roller burnishing simulation

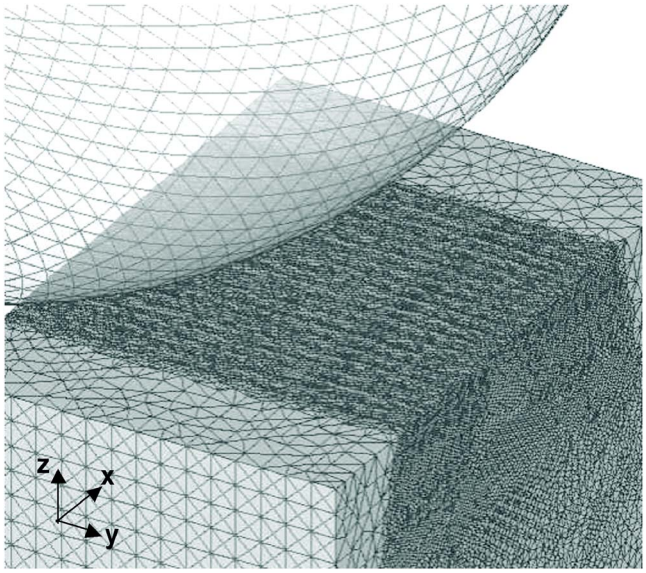

Fig. 8 Meshes of the ball tool and the workpiece in the 3D roller burnishing simulation

In the established 2D model, the ball movement was controlled by displacement. For every indentation cycle, the ball moved toward the workpiece until reaching the same maximum penetration depth and then unloaded from the workpiece (see Fig. 6). This maximum ball penetration was established from the results of 3D roller burnishing simulations of a single rolling path with DEFORM™-3D. Mesh density of the workpiece and the ball in 3D FEM model is shown in Fig. 8. The workpiece object has 190,000 tetrahedral elements with minimum element size of 25 μm at the surface. In the 3D model, the ball tool moves along y direction and rotates around its x-axis. Other settings and assumptions used for this 3D model are shown in Table 3.

The maximum penetration depth was obtained by conducting three 3D simulations at three different penetration depths to construct the predicted load versus ball penetration depth curve, as shown in Fig. 9. For the given burnishing pressure and Eq. (4), the

Table 3 Setup in the 3D FEM roller burnishing model

Object type:	Elastic-plastic workpiece rigid tool
Workpiece size	$2\times2\times3$ mm
Friction	$m=0$ (rolling+lubricant)
Thermal condition	Isothermal (coolant)
Initial roughness	Mean roughness depth, R_z, measured with stylus profiler
Tool movement	Tool moves toward the workpiece+rotates at the same tangential speed.
Burnishing force (F_b)	Controlled by the fluid pressure and calculated by Eq. (4)

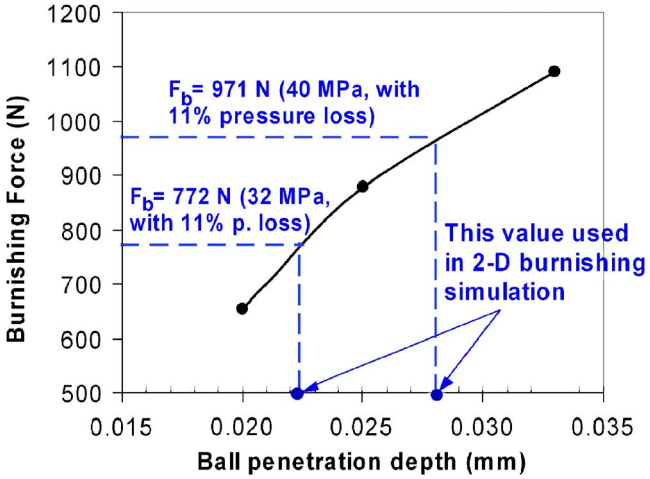

Fig. 9 Burnishing force versus depth curve, obtained from 3D roller burnishing simulations

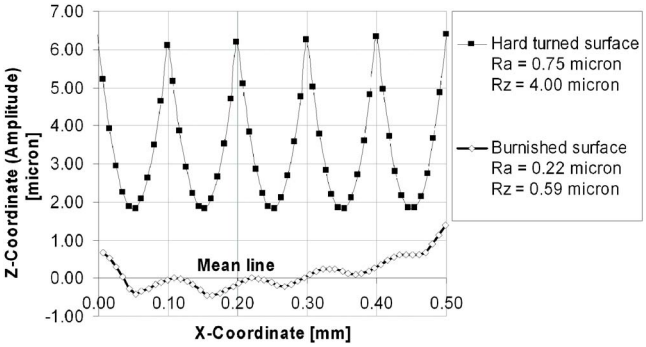

Fig. 11 Surface nodes of initial hard turned and burnished surfaces obtained from a 2D simulation (a burnishing condition uses P_b=40 MPa and f_b=0.05 mm/rev)

burnishing force can be calculated. The corresponding maximum ball penetration depth can be found from Fig. 9. Maximum ball penetration depths for the given burnishing pressure of 40 MPa and 32 MPa are 0.028 mm and 0.022 mm, respectively.

Although zero friction was assumed by the fact that pressurized fluid acts as coolant and lubricant, a series of 3D burnishing simulation were conducted to understand the effect of friction condition in the estimation of maximum ball penetration depth. Figure 10 shows the predicted force from the 3D FEM simulations using the same interference depth of 0.028 mm but different shear friction factors (m from $\tau=mk$, where τ is shear friction and k is shear flow stress of the workpiece material). The results show that friction factor has no effect on normal force (or burnishing force), which indicates that assumed friction condition does not affect the estimation of maximum penetration depth for the 2D model.

The movement of the ball in the simulation can be controlled by using two different ball movement controls, i.e., displacement control and force control. In the displacement control, the ball moves down and presses on the workpiece surface until reaching a maximum penetration depth for every indentation cycle. In the force control, the ball presses on the workpiece until reaching the maximum applied load for every indentation cycle. The limitation of the force control method used by Röttger [2] is that the final penetration depth of the ball under the plane strain condition (i.e., line contact) is actually smaller than it should be under the realistic 3D condition with the same applied force. Thus, it is more reasonable to use displacement control method in the 2D FEM model.

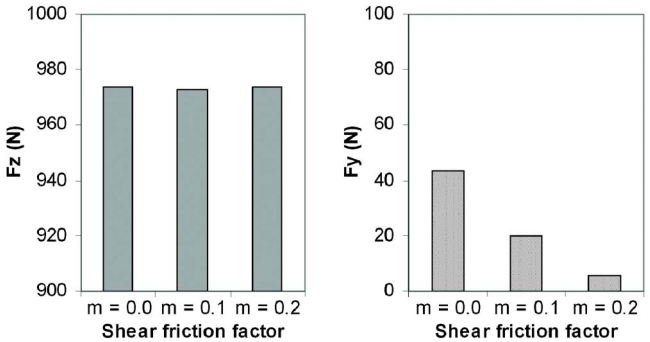

Fig. 10 Effect of friction factor on normal and rolling forces (in z and y directions)

In conducting the simulations, the following burnishing conditions were used:

- Burnishing ball diameter (d_b)=6 mm
- Burnishing pressure (p_b)=32 MPa, 36 MPa, 40 MPa
- Burnishing speed (v_b)=150 m/min
- Burnishing feed rate (f_b)=0.02 mm/rev, 0.05 mm/rev, 0.08 mm/rev

The initial machined surface roughness for the workpiece model was obtained from experimental measurement instead of theoretical calculation that was determined from nose radius and turning feed by Yen et al. [1] and Röttger [2]. As shown in Fig. 7, the distance between two roughness peaks is 0.1 mm (equivalent to the turning feed) and the measured roughness depth (R_z) or peak-to-valley roughness is 0.004 mm. Figure 7 also displays the displacement constraints that were applied on the left, right, and bottom boundaries of the workpiece. In Röttger [2], only four simulation cycles were used. However, the proposed model uses 11 simulation cycles in order to take into account the full deformation history of a single surface asperity during burnishing when the burnishing feed rate of 0.05 mm/rev is used. The total distance of the deformation zone in the simulation is 0.5 mm. For the burnishing feed rates of 0.02 mm/rev and 0.08 mm/rev, the numbers of simulation cycles were 26 and 7, respectively, in order to produce the equivalent deformation distance of 0.5 mm.

5 Simulation Results and Discussions

5.1 Data Extraction From FEM Roller Burnishing Simulation. After the simulation was completed, the geometry of the workpiece object was exported as a tabulated set of (x, z) coordinates of the boundary nodes. The node coordinates where the surface was indented by the ball tool were magnified and plotted in Fig. 11. Typical standard parameters used to describe the surface topography are the mean roughness R_a and the roughness depth R_z. A MAPLE code was created in order to read node coordinate data and calculate these surface parameters. First, a mean line was estimated by drawing a line that divides areas beneath the surface profile equally between positive and negative regions (see Fig. 11). Mean roughness and roughness depth can be calculated using Eqs. (5) and (6), respectively. Roughness depth R_z was calculated by taking an average of $Z_i=\max(z_i)-\min(z_i)$ for every interval of 0.1 mm of the burnished surface profile

$$R_a = \frac{1}{l}\int_0^l |z(x)|dx \tag{5}$$

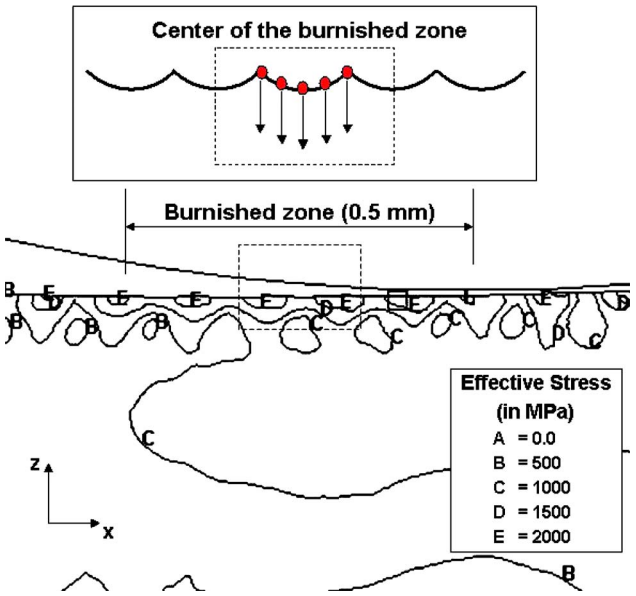

Fig. 12 Surface nodal points for extraction of residual stress data from 2D simulation (P_b=40 MPa and f_b=0.05 mm/rev)

$$R_z = \frac{1}{N}(Z_1 + Z_2 + Z_3 + \cdots + Z_N) \tag{6}$$

where

l=sampling or evaluation length (=0.5 mm in this study)
N=number of interval
Z=vertical distance of the highest to the lowest profile point

The effective stress contour, in Fig. 12, shows that high effective residual stresses predicted by 2D FEM simulations are mostly located in the local areas beneath the roughness peaks. This means there is a large variation of the stress from peak to valley positions of the surface profile. In addition, residual stress measurements with x-ray diffraction were conducted at the surfaces of an unknown position (i.e., peak, valley, or between them).

In order to obtain reasonable representative residual stress distributions from 2D simulations, the residual stress distributions over the depths along five points at the middle of the burnished zone were extracted and the average residual stresses were taken. Stresses in x direction represent axial stress while stresses in y direction represent tangential stress. Residual stresses in the radial direction (z direction) are small and negligible. For instance, the averaged residual stress distributions (i.e., tangential and axial stresses) from 2D simulations were plotted and compared to those of x-ray measurements in Fig. 13, (for P_b=40 MPa and f_b =0.05 mm/rev). Also in Fig. 13, both FEM simulation and experiment showed that roller burnishing induces compressive residual stress into the workpiece surface.

5.2 Effects of Burnishing Feed Rate on Surface Properties. Figure 14 shows the effects of burnishing feed rate on surface roughness parameters R_a and R_z, at the same burnishing pressure (P_b=40 MPa). Also in Fig. 14, the results predicted by 2D FEM simulations and those obtained from experiments are shown. It should be noted in Fig. 14 that, as burnishing feed increases, mean roughness R_a also increases. This is because the distance between successive burnishing ball traces increases with the burnishing feed, and thus, there is less chance for the ball to smooth out all the edges of the irregularities.

To obtain a smoother surface by burnishing, the burnishing feed

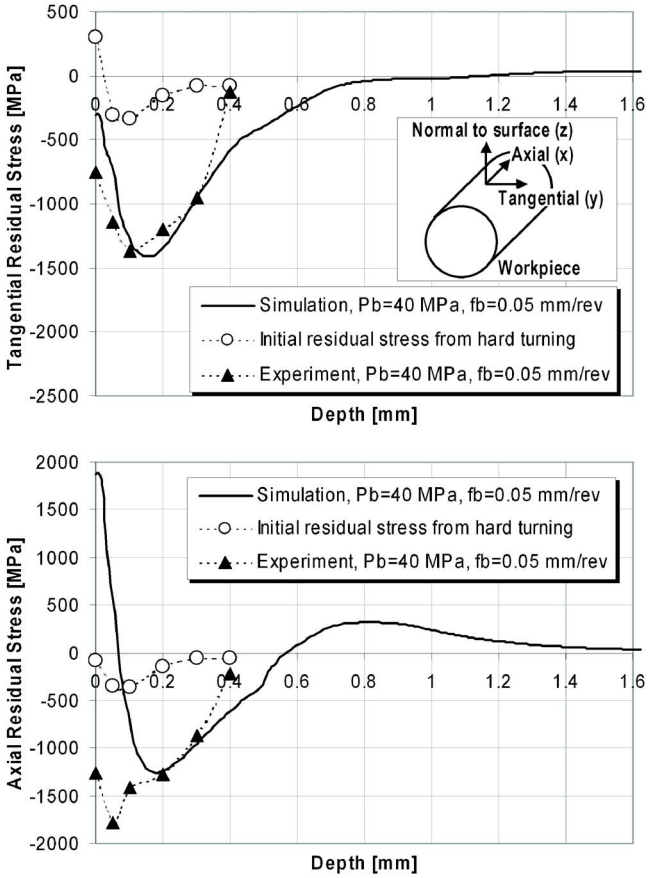

Fig. 13 Tangential and axial residual stress distributions of the hard turned and the burnished surfaces (from simulation and experiment), for P_b=40 MPa and f_b=0.05 mm/rev

should be smaller than the turning feed. This is because, if the same or higher burnishing feed is used, then the tool's rolling motion can be parallel to the feed grooves of the turned surface. Hence, burnishing ball will rather push surface valleys lower and increase surface roughness instead of smoothen the surface ridges. On the other hand, if a very small burnishing feed is used, then the tool has more chances to flatten the surface peaks and produce a greater amount of plastic deformation on the workpiece surface due to overlapping of successive ball traces.

Compared to hard turned surface that has R_a=0.75 μm and R_z=4 μm (in Fig. 11), the roller burnished surface has less roughness for all different burnishing feed rates used in this study (in Fig. 14). This surface roughness improvement is shown in FEM simulations as well as in the experiments.

The variation of surface roughness parameters (R_a and R_z) over different feed rates from 2D FEM simulations showed the same trend as experimental results (Fig. 14). However, simulations show reasonable agreement only for the mean roughness R_a and significant difference for the roughness depth R_z. This difference may be due to the combination of several factors, i.e., (i) the numerical error produced during FEM calculations, (ii) the plane strain assumption (whereas roller burnishing process is a 3D process in nature), and (iii) the fact that FEM model cannot consider the influence of stiffness and dynamics of the machine tool and workpiece setup. In addition, the element size may also affect the predicted results.

With the present computational capability, 2D FEM simulations provided only qualitative results in predicting the surface roughness parameters, especially in the case of the mean roughness.

Figure 15 shows that 2D simulations predict the tangential residual stress distributions in good agreement with experimental

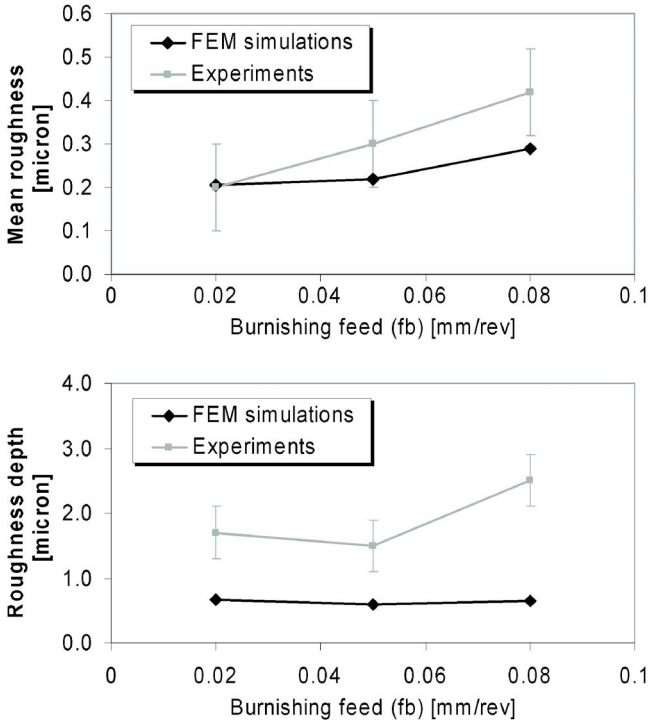

Fig. 14 Effects of burnishing feed rate (for the same burnishing pressure of 40 MPa) on mean roughness and roughness depth

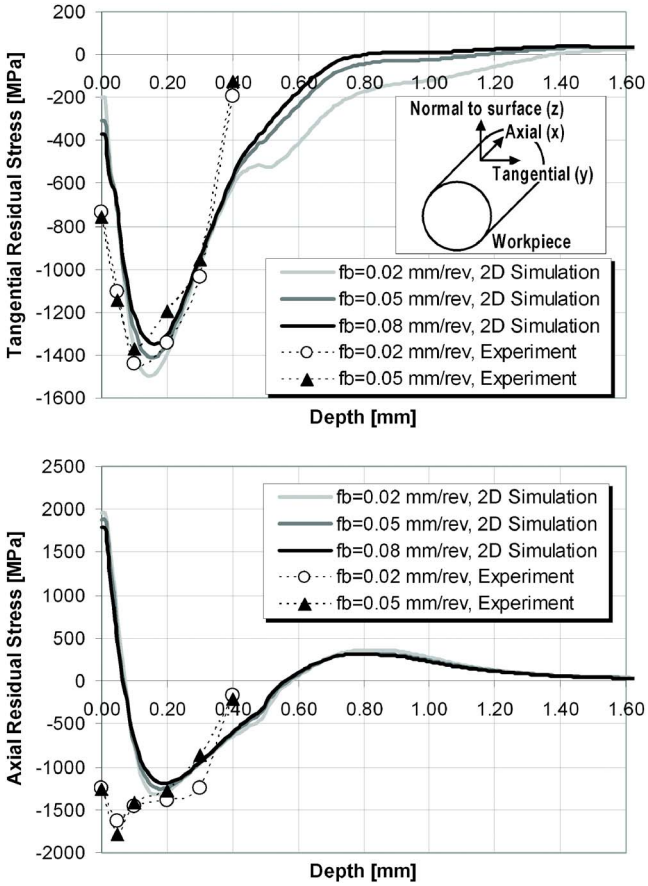

Fig. 15 Effects of burnishing feed rate (for the same burnishing pressure of 40 MPa) on tangential and axial residual stress distributions along the depth (distance from surface)

results. Maximum compressive residual stress values are matched, with 4% difference. The effective depths that contain compressive residual stress predicted by the simulations are slightly larger than the results from experiments. However, FEM simulation cannot predict compressive residual stresses in axial direction, at and near the burnished surface (from the depth of 0 to 0.1 mm). Tensile residual stresses predicted from the simulation are due to the plane strain assumption used in the 2D model since the tool is presented as a cylindrical object rather than a spherical object. Line contact is presumed in the 2D FEM simulation rather than point contact that is typically generated by spherical tool. In the 2D model, the tool geometry, which is assumed to be larger in axial direction, pushes more material to flow aside and generates more tensile stresses in axial direction than what is expected from a spherical tool. Nevertheless, the axial residual stresses beyond 0.2 mm depth match well with the experiments.

According to FEM simulation results in Fig. 15, a decrease in burnishing feed slightly raises the magnitude of the compressive residual stresses in both axial and tangential directions. This can be explained by the fact that a small feed indicates shorter distance between ball traces. As a result, the workpiece surface was subjected to greater amount of plastic deformation and residual stresses due to more repetitive compression by the ball tool. Simulations showed greater influence of burnishing feed rate on tangential residual stresses (i.e., more variation of residual stresses in tangential direction due to change in burnishing feed). The effects of feed rate on residual stresses are consistent with experimental observations.

5.3 Effects of Burnishing Pressure on Surface Properties. The effects of burnishing pressure on surface roughness are shown in Fig. 16. The values of mean roughness R_a predicted by FEM simulations reasonably agree with the experimental results. FEM simulations showed that the mean roughness decreased when higher burnishing pressure was used. However, unlike the experimental observations, FEM simulations did not show the trend that there was almost no improvement of surface finish when using burnishing pressure higher than 36 MPa.

The value of roughness depth R_z predicted by FEM simulation also decreased as the burnishing pressure increased from 32 MPa to 36 MPa. However, further increase in the burnishing pressure up to 40 MPa causes higher roughness depth, which means that, for the given material and hardness, there is an optimum burnishing pressure for the best surface finish between 32 MPa and 40 MPa. Surface finish predictions by FEM simulations have the same trend as those of experiments but show considerable difference in the roughness depths. Only qualitative results of surface roughness can be provided through FEM simulations.

Similar to Sec. 5.2, the quantitative differences may be explained by (i) the numerical error produced during FEM calculations, (ii) the 2D plane strain assumption, and (iii) the influence of stiffness and dynamics of machine tool and workpiece setup.

Figure 17 shows the distributions of the residual stresses when using different burnishing pressures and the same burnishing feed rate. Also in Fig. 17, 2D simulations predict the tangential residual stresses in good agreement with the experimental results. Maximum compressive residual stress values are matched, within 11%. The effective depths that contain compressive residual stress from the simulations are slightly larger than the experiments (when comparing 0.55 mm from the simulation and 0.4 mm from experiments).

Similar to previous section, 2D simulations cannot predict compressive residual stresses in axial direction and at the burnished surface (from the depth of 0 to 0.1 mm). Nevertheless, the trends in residual stresses in function of burnishing pressure qualitatively agree with the experiments, where higher burnishing pressures generate more compressive residual stress near the surface and

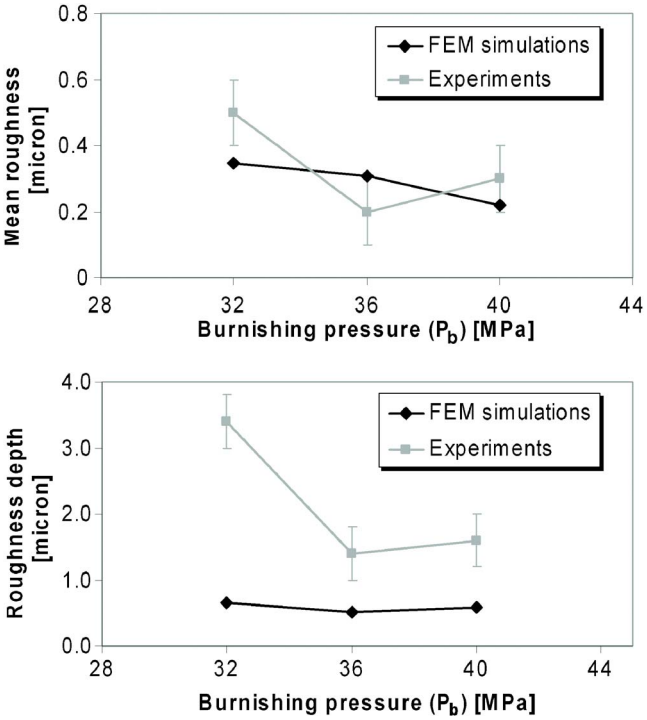

Fig. 16 Effects of burnishing pressure (for the same burnishing feed rate of 0.05 mm/rev) on mean roughness and roughness depth

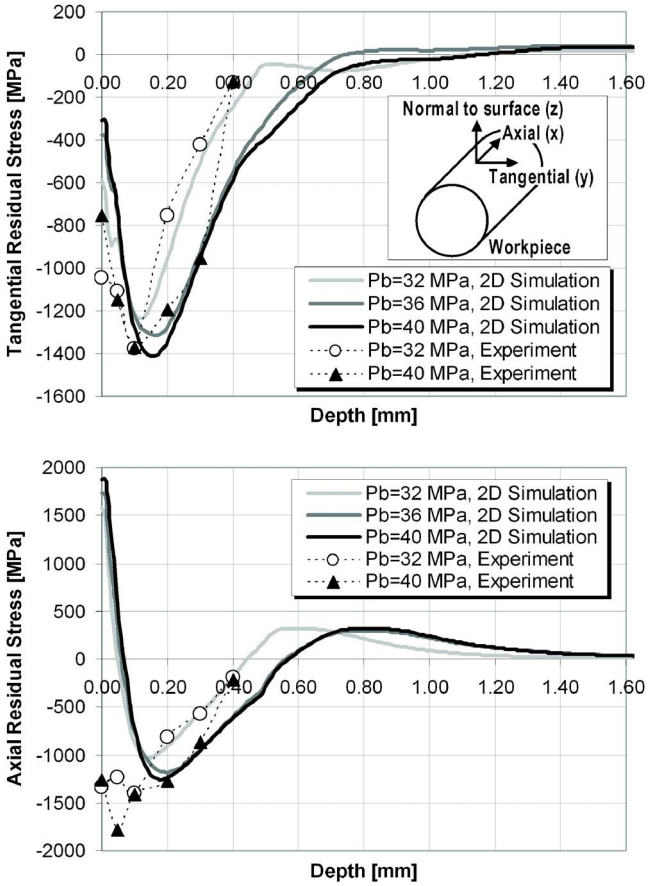

Fig. 17 Effects of burnishing pressure (for the same burnishing feed rate of 0.05 mm/rev) on tangential and axial residual stress distributions along the depth (distance from surface)

produce a deeper effective compressive stress layer. In addition, the location of maximum compressive residual stresses moves deeper into the surface with increasing burnishing pressure, (at ~0.15 mm for P_b=32 MPa and at 0.2 mm for P_b=36 MPa in Fig. 17).

The increase of burnishing pressure (or applied burnishing force) leads to an increase in the amount of plastic deformation as more roughness valleys are "filled" during the process. This leads to an increase in the compressive stresses applied to the surface, which in turn increase the surface hardness and compressive residual stresses as observed in this study and the study by Klocke and Liermann [3].

5.4 Effect of Initial Residual Stresses Generated by Hard Turning. In the actual experiment, hard turning was performed prior to roller burnishing. Residual stresses produced by hard turning may or may not influence the residual stress state after burnishing. This can be studied using 2D FEM model by incorporating the measured residual stresses of the hard turned surface (as shown in Fig. 13).

A number of MATLAB codes were written to read the tabulated data of residual stress measurements (i.e., residual stress at different depths) and convert them into the stress component data for each mesh element of the workpiece object in FEM model. This was done by calculating the center coordinate (X_{center}, Z_{center}) of each quadratic mesh element from the shape function for the bilinear four node square element using Eq. (7) and (8). The stress components of each element was estimated from the given Z_{center} coordinate and the measured residual stresses from Fig. 13, using spline-line interpolation

$$\{x\} = \sum_{a=1}^{4} (\xi, \eta)\{x_a\}^e \tag{7}$$

$$N_a = \tfrac{1}{4}(1 + \xi_a \xi)(1 + \eta_a \eta) \tag{8}$$

where

x_a=node coordinates in real space
N_a=shape functions for bilinear four node element
ξ_a, η_a=node coordinates in the natural space

Initial residual stresses, in tangential and axial directions, after hard turning and prior to 2D burnishing simulation, are illustrated in Fig. 18. A 2D roller burnishing simulation with initial stress data was conducted at P_b=32 MPa and f_b=0.05 mm/rev. Re-

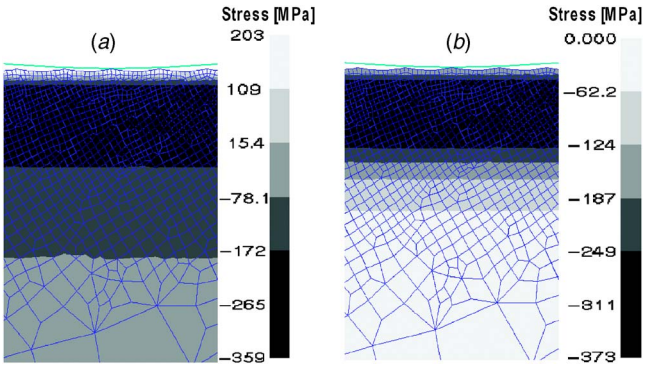

Fig. 18 Residual stress of hard turned surface, assigned in the workpiece mesh model of 2D roller burnishing simulation: (*a*) tangential residual stress and (*b*) axial residual stress

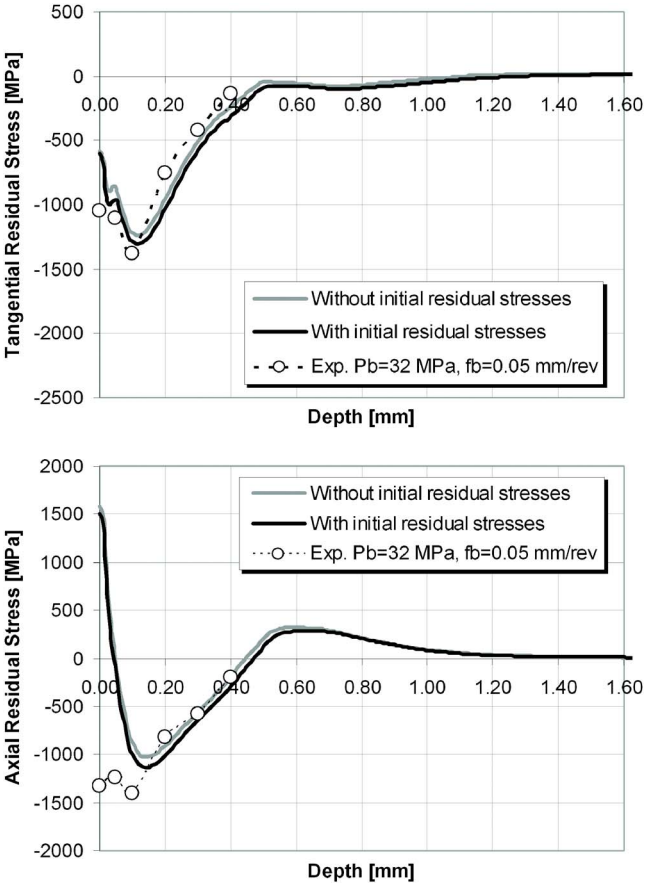

Fig. 19 Effects of initial residual stresses from hard turning in the predicted residual stresses in 2D roller burnishing simulation, for P_b=32 MPa, f_b=0.05 mm/rev

sidual stress results from this simulation were compared to other simulations that were modeled without initial stress as well as the experimental measurements, as shown in Fig. 19.

The results show that the initial residual stresses from hard turning have insignificant effect on the residual stresses obtained after roller burnishing for the range of burnishing pressures used in this study. This could be explained by the fact that the minimum burnishing pressure used in this study (32 MPa) had sufficient force to press the surface into a certain depth and could suppress all the residual stresses previously generated by hard turning. According to experimental study in [2], although high tensile residual stresses were produced by turning with a worn tool, the residual stress after burnishing were still compressive and not different from those obtained from turning with a sharp tool.

6 Summary and Conclusions

In this study, two main tasks were conducted: (i) improvements of the FEM roller burnishing model [1] and (ii) FEM simulations to analyze the effects of roller burnishing parameters by using the conditions selected for the experiments. For the modifications of the existing FEM model in [1], the flow stress model from ball indentation tests, the influence of pressure loss during roller burnishing operation, and the actual roughness of the hard turned surface were considered. A workpiece size of 7×6 mm was used in the 2D FEM model since the predicted surface roughness and residual stresses were not affected by the displacement boundary constraints. A 3D roller burnishing model of one rolling path was conducted to calculate the maximum ball penetration depth for use in a 2D FEM model. This allowed one to have more reliable predictions near the surface and more realistic tool/workpiece contact.

The effects of roller burnishing parameters can be summarized as follows:

1. As burnishing feed rate f_b increases, surface roughness increases. If a very high feed value is used, then the tool has less chance to flatten the roughness peaks.
2. FEM simulations can predict only mean roughness R_a but not roughness depth R_z. Overall, they can provide only a qualitative trend of surface roughness for different process conditions. This error may be due to the assumptions of 2D plane strain and the fact that FEM simulation cannot consider the dynamics of machine/workpiece setup.
3. Burnishing pressure has the most important effect in surface roughness. Both FEM and experiments show that higher burnishing pressure (40 MPa) produces better surface finish.
4. Predictions of residual stress distributions beneath the burnished surface, with the 2D FEM model are in good agreement with the experimental measurements obtained using x-ray diffractions.
5. Residual stresses are influenced slightly by the burnishing feed rate. Both FEM simulation and experiment show that increasing burnishing feed rate causes a slight decrease in residual stresses.
6. Burnishing pressure has the most influence on residual stresses. The amount of plastic deformation in the workpiece increases, and hence, the magnitude of compressive residual stresses increase with increasing burnishing pressure. Experimental results and FEM predictions for the residual stresses at different burnishing pressures are in good agreement.
7. Initial residual stress produced by hard turning has an insignificant effect on the residual stress predicted in roller burnishing simulation.

Future work on roller burnishing research should consider the following:

1. Conducting additional 2D burnishing simulations to understand the effects of the ball diameter
2. The use of a statistical approach to model the surface roughness parameters since the effects of roller burnishing parameters on surface roughness was obtained only qualitatively by means of 2D FEM simulations
3. The use of the developed FEM technique to optimize practical burnishing processes in producing industrial parts

Acknowledgment

This study was conducted at the ERC/NSM with support from the NSF Grant No. DMII-0323631. This support is gratefully acknowledged. The authors would like to thank also to Dr. Mahen Patel for allowing us to conduct hard turning and roller burnishing experiments at Hardinge Inc., and the Timken Company for making residual stress measurements.

Nomenclature

d_b = ball diameter
E = Young's modulus
ε_p = plastic strain
F_b = burnishing force
f_b = burnishing feed rate
l = sampling or evaluation length for surface roughness measurement (which is 0.5 mm in this study)
N = numbers of intervals considered for surface roughness measurement
N_a = shape functions for bilinear four node element

n = strain-hardening exponent
η_a = node coordinates in the natural space
P_b = applied fluid pressure
R_a = mean roughness
R_z = roughness depth
σ = flow stress
$\bar{\sigma}$ = effective stress
$\sigma_{r,a}$ = axial residual stress
$\sigma_{r,t}$ = tangential residual stress
σ_x = stress in x direction
σ_y = stress in y direction
σ_y = yield stress
v_b = burnishing speed
W = plane that pass through the center of the ball along one roughness ridge
x_a = node coordinates in real space
ξ_a = node coordinates in the natural space
Z = vertical distance of the highest to the lowest profile point of the surface

References

[1] Yen, Y. C., Sartkulvanich, P., and Altan, T., 2005, "Finite Element Modeling of Roller Burnishing Process," CIRP Ann., **54**, pp. 237–240.
[2] Röttger, K., 2002, "Walzen hartgedrehter Oberflaechen," Ph.D. dissertation, WZL, RWTH Aachen, Germany.
[3] Klocke, F., and Liermann, J., 1998, "Roller Burnishing of Hard Turned Surfaces," Int. J. Mach. Tools Manuf., **38**(5-6), pp. 419–423.
[4] ECOROLL AG Werkzeugtechnik, 1996, "Application Description: Deep Rolling," ECOROLL AG Research *Report No.* AO-4088/1E, pp. 1–15.
[5] Luca, L., 2002, "Investigation Into the Use of Ball Burnishing of Hardened Steel Components as a Finishing Process," Ph.D. dissertation, University of Toledo.
[6] Prevéy, P. S., Ravindranath, R. A., Shepard, M., and Gabb, T., 2003, "Case Studies of Fatigue Life Improvement Using Low Plasticity Burnishing in Gas Turbine Engine Applications," *Proceedings of ASME Turbo Expo*, June 16–19, Atlanta, ASME, New York.
[7] Hassan, A. M., and Maqableh, A. M., 2000, "The Effects of Initial Burnishing Parameters on Non Ferrous Components," J. Mater. Process. Technol., **102**, pp. 115–121.
[8] El-Axir, M. H., and El-Khabeery, M. M., 2003, "Influence of Orthogonal Burnishing Parameters on Surface Characteristics for Various Materials," J. Mater. Process. Technol., **132**, pp. 82–89.
[9] Némat, M., and Lyons, A. C., 2000, "An Investigation of the Surface Topography of Ball Burnished Mild Steel and Aluminum," Int. J. Adv. Manuf. Technol., **16**, pp. 469–473.
[10] Shiou, F. J., and Chen, C. H., 2003, "Determination of Optimal Ball Burnishing Parameters for Plastic Injection Moulding Steel," Int. J. Adv. Manuf. Technol., **3**, pp. 177–185.
[11] Prevéy, P. S., 2000, "The Effect of Cold Work on the Thermal Stability of Residual Compression in Surface Enhanced IN718," *Proc. of 20th ASM Materials Solutions Conference & Exposition*, St. Louis, Missouri, Oct. 10–12, ASM, Metals Park, OH, pp. 1–9.
[12] Prevéy, P. S., and Cammett, J., 2000, "Low Cost Corrosion Damage Mitigation and Improved Fatigue Performance of Low Plasticity Burnished 7075-T6," *Proc. of 4th International Aircraft Corrosion Workshop*, Solomons, MD, Aug. 22–25.
[13] Prevéy, P. S., Telesman, J., Gabb, T., and Kantzos, P., 2000, "FOD Resistance and Fatigue Crack Arrest in Low Plasticity Burnished IN718," *Proc. of 5th National Engine High Cycle Fatigue Conference*, Chandler, AZ, Mar. 7–9.
[14] Prevéy, P. S., Shepard, M. J., and Smith, P. R., 2001, "The Effect of Low Plasticity Burnishing (LPB) on the HCF Performance and FOD Resistance of Ti-6Al-4V," *Proc. of 6th National Turbine Engine High Cycle Fatigue (HCF) Conference*, Mar. 5–8, Jacksonville, FL.
[15] Prevéy, P. S., Ravindranath, R. A., Shepard, M., and Gabb, T., 2003, "Case Studies of Fatigue Life Improvement Using Low Plasticity Burnishing in Gas Turbine Engine Applications," *Proc. of ASME Turbo Expo*, June 16–19, Atlanta, ASME, New York.
[16] Hassan, A. M., and Al-Bsharat, A. S., 1996, "Influence of Burnishing Process on Surface Roughness, Hardness, and Microstructure of Some Non-Ferrous Metals," Wear, **199**, pp. 1–8.
[17] Hassan, A. M., and Maqableh, A. M., 2000, "The Effects of Initial Burnishing Parameters on Non-Ferrous Components," J. Mater. Process. Technol., **102**, pp. 115–121.
[18] Hassan, A. M., Al-Jalil, H. F., and Ebied, A. A., 1998, "Burnishing Force and Number of Ball Passes for the Optimum Surface Finish of Brass Components," J. Mater. Process. Technol., **83**, pp. 176–179.
[19] Bouzid, W., Tsoumarev, O., and Saï, K., 2004, "An Investigation of Surface Roughness of Burnished AISI 1042 Steel," Int. J. Adv. Manuf. Technol., **24**, pp. 120–125.
[20] Black, A. J., Kopalinsky, E. M., and Oxley, P. L. B., 1997, "Analysis and Experimental Investigation of a Simplified Burnishing Process," Int. J. Mech. Sci., **39**(6), pp. 629–641.
[21] Skalski, K., Morawski, A., and Przybylski, W., 1995, "Analysis of Contact Elastic-Plastic Strains During the Process of Burnishing," Int. J. Mech. Sci., **37**(5), pp. 461–472.
[22] Bouzid, W., and Saï, K., 2004, "Finite Element Modeling of Burnishing of AISI 1042 Steel," Int. J. Manu. Tech., **25**, pp. 460–465.
[23] Morris, E., Cho, H., Sartkulvanich, P., and Altan, T., 2005, "Determining the Flow Stress at the Surface of Materials Using Indentation Testing With Conical or Spherical Indenters," ERC thesis Report No. HPM/ERC/NSM-05-R-25, The Ohio State University, Columbus.
[24] Caccialupi, A., 2003, "Systems Development for High Temperature, High Strain Rate Material Testing of Hard Steels for Plasticity Behavior Modeling," MS thesis, Georgia Institute of Technology, Atlanta, GA.